The 14th International Topical Meeting on Nuclear Reactor Thermalhydraulics, NURETH-14
Toronto, Ontario, Canada, September 25-30, 2011

NURETH14-482

LARGE-EDDY SIMULATION OF SINGLE-PHASE PRESSURIZED THERMAL SHOCK

M.S. Loginov[1], A. Shams[1], E.M.J. Komen[1], and T. Höhne[2]

[1] Nuclear Research and Consultancy Group (NRG), 1755 ZG Petten, the Netherlands
[2] Forschungszentrum Dresden-Rossendorf (FZD), 01328 Dresden-Rossendorf, Germany

Abstract

Pressurized Thermal Shock (PTS) is identified as one of the safety issues where Computational Fluid Dynamics (CFD) can bring real benefits. Turbulence modeling may impact the overall accuracy of the calculated thermal loads on the Reactor Pressure Vessel (RPV) walls. Therefore advanced methods for turbulent flows are required. In the current paper, we summarize our efforts on large-eddy simulations (LES) of a complex turbulent mixing in the RPV. First, the mesh resolution is investigated, and a comparison procedure is established. The analysis have shown necessity of comparison in both time and frequency domains. Next, a validation against experiment is performed using three cases with different flow rates in the primary loop. The validation results have successfully reproduced the flow patterns and have shown good quantitative agreement for the near-wall temperature drop.

1 Introduction

Pressurized Thermal Shock (PTS) in general denotes the occurrence of thermal loads on the Reactor Pressure Vessel (RPV) under pressurized conditions, i.e. in Pressurized Water Reactor (PWR). These thermal loads may lead to very large stresses and to the instability of possible flaws present inside the RPV wall. Therefore, assessment of PTS is important for long term operation, since the integrity of the RPV has to be assured throughout the lifetime of the reactor. The most severe PTS scenario limiting the RPV lifetime is a cold water Emergency Core Cooling (ECC) injection into the cold leg during a Loss-Of-Coolant Accident (LOCA). The injected cold ECC water mixes with the hot fluid present in the cold leg, and the resulting mixture flows towards the downcomer where further mixing takes place. When the cold water comes into contact with the RPV wall, it leads to large temperature gradients and consequently to very high stresses in the walls.

The existing thermal-hydraulic system codes currently applied for this problem are based on simplified one-dimensional flow representations. These codes cannot predict the complex three-dimensional flows occurring during the ECC injection. On the other hand, Computational Fluid Dynamics (CFD) can be used to model these phenomena including the effect of turbulence. Improved CFD codes are expected to be used extensively for PTS analysis within the framework of

long term operation of nuclear power plants. Indeed, PTS has received the highest priority among safety issues for which CFD can bring real benefits [1].

Almost all CFD simulations performed in the past use the transient Reynolds-Averaged Navier-Stokes (RANS) approach. The transient RANS simulations have shown that the thermal stratification in the cold legs of the UPTF and ROCOM facilities were predicted accurately [2]. However, it was less capable of grasping the complex oscillating flow in the downcomer. One of the possible reasons for the discrepancies in the downcomer could be the inherit limitations of RANS method for the complex buoyancy-driven flow in the downcomer. Consequently, more advanced CFD methods like Large Eddy Simulation (LES) may be required to resolve the turbulent flow and heat transfer accurately.

In this paper a summary of our experience on the LES modeling of single-phase PTS is presented. Initially, we performed a grid resolution study and established a validation procedure. Afterwards, a validation against an experiment is provided. These efforts are described in the following sections. First, the experimental and numerical setup is shown. The grid resolution study and challenges for validation are explained in the next section. Subsequently, the validation of the model against experimental data is shown. Finally, the accuracy of LES for single-phase PTS is discussed.

2 Experimental and numerical setup

2.1 ROCOM experimental facility

The ROCOM mixing facility (Fig. 1) represents the primary system of a KONVOI type of reactor on a 1:5 linear scale [3]. The original RPV is modeled by a transparent plexiglas model. The following internals of the reactor pressure vessel are included: a core barrel with lower support plate and core simulator, a perforated drum in the lower plenum, and the inlet/outlet nozzles. In the ROCOM facility, the RPV is connected to four circulation loops with a pump in each loop. The pumps are individually controlled by frequency transformers. The volume of the loops is scaled (1:125) according to the linear scaling of the RPV with respect to the original KONVOI reactor. The temperature variation is modeled through the adjusted density. The ECC injection is represented by injection of water with sugar added to increase the density of the colder ECC water. Additionally, the ECC water is labeled by a very small amount of salt. The salt has no further influence on the density, although it significantly changes the conductivity of the water, which can be measured. In the facility, so-called wire mesh sensors are applied [4]. To measure the changes in conductivity, and therewith the mixing of the injected ECC water, four wire mesh sensors are used in the model. The sensors enable a high resolution sampling of the concentration field in the RPV in both space and time.

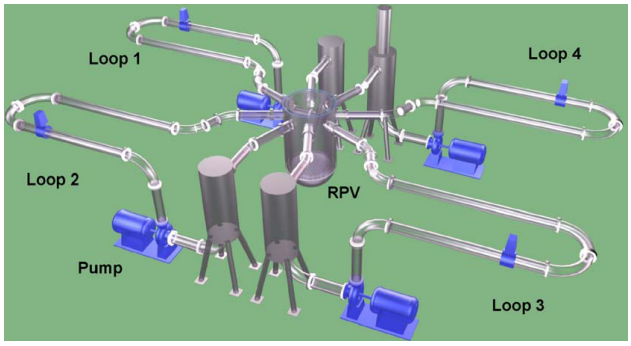

Figure 1: ROCOM experimental facility with four loops and flow circulation pumps.

Table 1: The ROCOM test cases.

case	Q, m^3/h	U_b, m/s	*Re*	N_r	flow type
5%	9.8	0.154	26972	5	buoyancy-driven
10%	18.5	0.291	50912	5	transition
15%	27.8	0.437	76512	3	momentum-driven

2.2 Selected experiments

The grid resolution study is performed with the stagnant fluid in the RPV [5, 6]. The ECC fluid is injected during $40\ s$ with a mass flow rate of $1.47\ kg/s$, the density ratio between injected and stagnant fluid was $\rho_{ECC}/\rho = 1.05$. The primary loop pumps were switched off during the experiment, there is no co-flow in the cold leg. After finishing the ECC injection, the flow was driven purely by the buoyancy force.

Three buoyancy-related experiments [3] have been selected for the validation of the LES model. The ECC flow rate of $3.6m^3/hour$, the injection time of $10s$, and the same density ratio of 1.05 were kept the same for all three cases. The test cases differ with respect to the flow rate in the cold leg where the ECC injection takes place. They correspond to natural circulation at 5, 10 and 15% of nominal conditions. There was no flow in the other loops. The conditions in the cold leg with the ECC pipe are summarized in Tab. 1. In this table, the corresponding flow rate Q, bulk velocity $U_b = 4Q/\pi D^2$, Reynolds number $Re = U_b D/\nu$, number of experimental realizations N_r and the flow types accordingly to [3] are given. Here $D = 0.15m$ is diameter of the cold leg and $\nu = 8.57 \cdot 10^{-7}\ m^2/s$ is kinematic viscosity of the water in the primary loop. The densities of the primary and injected water were $\rho = 998\ kg/m^3$ and $\rho_{ECC} = 1050\ kg/m^3$ respectively.

2.3 CFD Model

In the current study we employ the same numerical approach as before [6], which is briefly summarized below. The incompressible formulation of the Navier-Stokes equations is used in the computational setup. The effect of the density differences on the flow phenomena is taken into account by the incorporated buoyancy force. In the applied numerical model, the filtered Navier-Stokes equations are solved in the following form [7]:

$$\frac{\partial \overline{\mathbf{u}}}{\partial t} + \nabla \cdot (\overline{\mathbf{u}} \otimes \overline{\mathbf{u}}) + \frac{1}{\rho}\nabla \overline{p} + \nabla \cdot (\mathbf{B} - 2\nu \mathbf{D}) = \mathbf{F}, \tag{1}$$

where $\overline{\mathbf{u}}$ is the filtered velocity, $\overline{p}$ is the filtered pressure, $\mathbf{F}$ is the buoyancy force, ρ is the density of the primary water initially present in the cold leg and RPV, and ν is the laminar viscosity. $\mathbf{D}$ and $\mathbf{B}$ denote symmetric part of the deformation tensor and subgrid-scale (SGS) stress tensor respectively. In the present simulations, a recently developed SGS model of [8] was employed. Equation (1) is supplemented by the transport equation for a filtered scalar $\overline{T}$:

$$\frac{\partial \overline{T}}{\partial t} + \overline{\mathbf{u}} \cdot \nabla \overline{T} = \Big(D_t + \frac{\nu_t}{Sc_t}\Big)\nabla^2 \overline{T}, \tag{2}$$

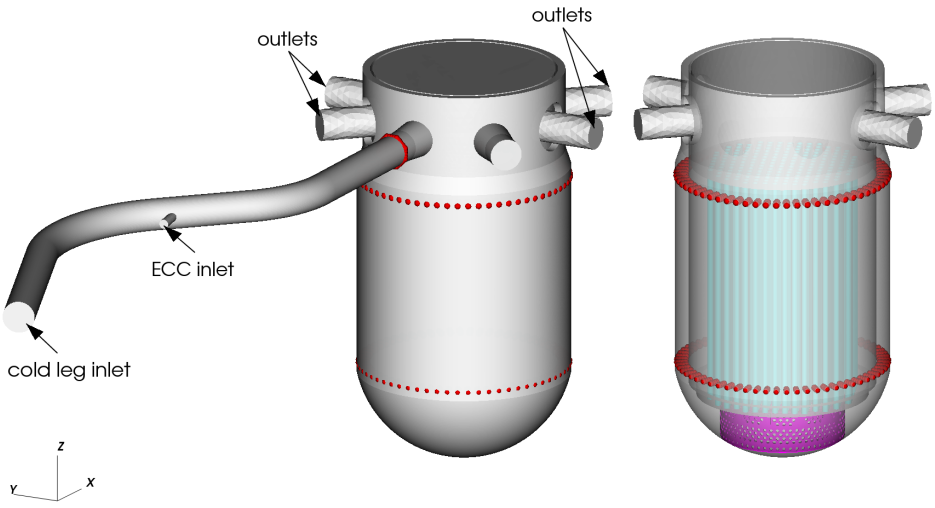

Figure 2: The computational domain and RPV internals.

where $D_t = 1.5 \cdot 10^{-9} m^2/s$ is the diffusion coefficient, and $Sc_t = 0.85$ is the turbulent Schmidt number. The scalar represents sugar concentration, normalized to the value at the ECC inlet. The buoyancy force $\mathbf{F}$ in Eqn. (1) resulting from the density difference is expressed in the following form:

$$\mathbf{F} = \mathbf{g}\left(\frac{\rho_m - \rho}{\rho_m}\right); \quad \rho_m = \rho + \overline{T}(\rho_{ECC} - \rho), \tag{3}$$

where $\mathbf{g} = 9.81 m/s^2$ is the gravity vector, ρ_{ECC} is the density of the injected ECC water, and ρ_m is the density of the mixture.

Eqns. (1) through (3) along with the incompressibility constraint are solved with a second-order central discretization scheme in space. For time, an implicit second-order backward-differencing scheme is used. Pressure is eliminated by solving the Poisson equations with a mixed SIMPLE/PISO velocity-pressure coupling algorithm. The applied code is based on standard numerical libraries [7].

Only the relevant part of the ROCOM facility is taken into account for the simulation domain. Namely, the RPV and the part of the cold leg with the ECC injection pipe are considered, as shown in Fig. 2. The RPV internals were simplified for grid resolution study, while detailed geometry of the perforated drum, core support plate, and core simulator, were reproduced very closely in for validation. The dots at the surface denote the positions of the experimental sensors. In the following, these measuring positions are referred to as “reactor inlet”, “upper downcomer” and “lower downcomer” sections.

The mesh consists primarily of hexahedral cells. Tetrahedral parts have been used near the connection of the ECC injection pipe with the cold leg and around the perforated drum in the lower plenum. The grid resolution is studied on coarse, medium and fine mesh (see grids **A**, **B** and **C**in

Table 2: The mesh sizes.

case	Δ_x mm	Δ_θ mm	Δ_n mm	total amount of cells in the domain
A	6.0	6.0	1.1	3.0×10^6
B	4.5	4.5	1.1	5.3×10^6
C	3.0	3.0	1.1	12.3×10^6
5%	7.7	3.1	1.5	13.2×10^6
10%	4.9	2.0	1.0	15.2×10^6
15%	3.6	1.4	0.7	19.9×10^6

Tab. 2). For each of the three experimental cases, a separate mesh has been generated with the recommended non-dimensional values for the cell size, the dimensional sizes are summarized in Tab. 2. A typical cell size of $4.5mm$ is used in the RPV for grid resolution study and for validation.

For the stagnant fluid in RPV the cold inlet was set as a wall. In validation simulations the instantaneous data for fully developed turbulent flow are provided at the cold inlet using a mapping technique with prescribed bulk velocity [9]. During the ECC injection, a fully developed turbulent profile (1/7 power law) was imposed for the velocity at the ECC inlet. Turbulent fluctuations at this position were approximated by adding a random noise with a magnitude of 2.5% of the mean velocity. The concentration T at the ECC inlet has unit value during the injection and zero otherwise. At the walls, the no-slip condition is used together with a standard wall function. Furthermore, a zero gradient condition is employed for the pressure and scalar. At the outlets, zero static pressure was specified, together with a zero gradient for the scalar.

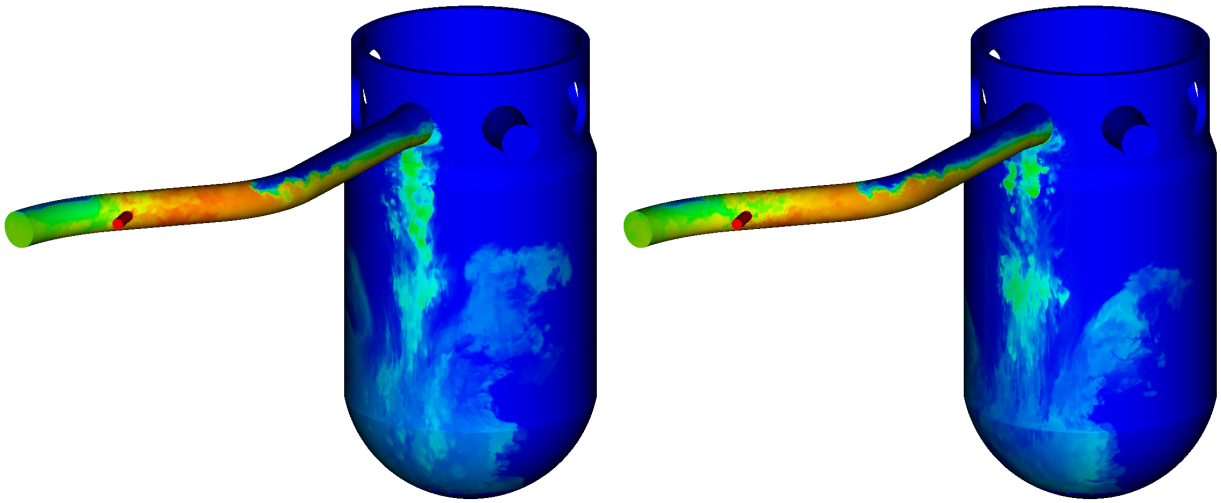

Figure 3: Distribution of concentration at the wall in different realizations at $t = 25.5\ s$.

3 Grid resolution assessment

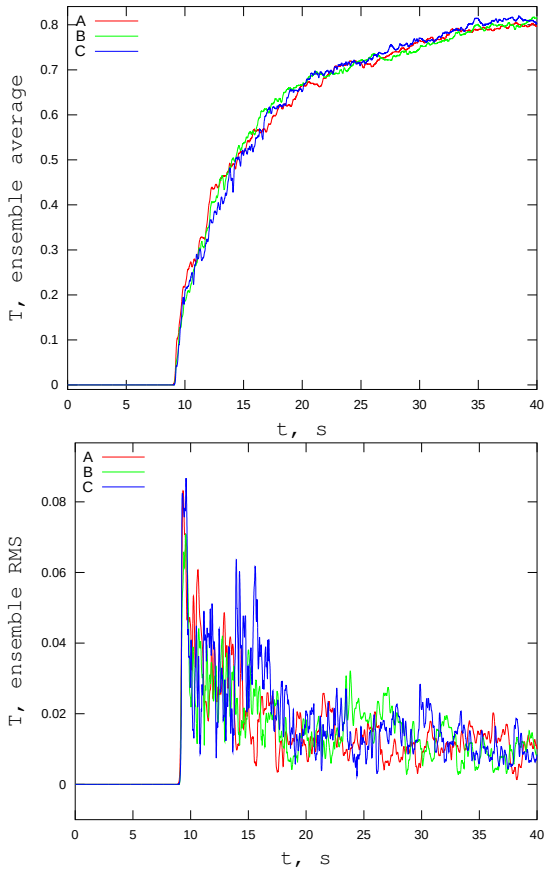

Figure 4: Ensemble average and RMS for the scalar on the different meshes.

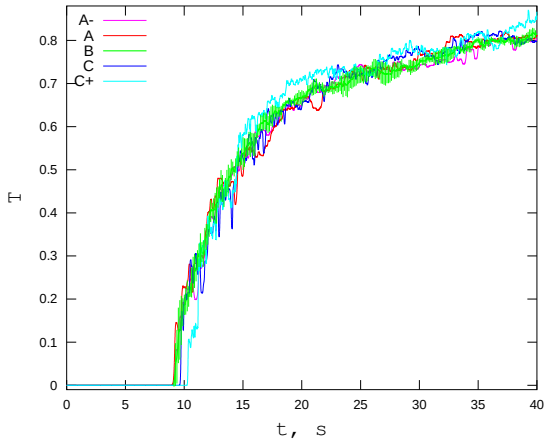

Figure 5: Solution for scalar concentration on the different meshes.

Analysis of the transient three-dimensional turbulent flow is a challenging task. A collection of instantaneous samples and obtaining turbulence characteristics (e.g., Reynolds stresses, integral length scale) is only possible for statistically steady-state conditions. The necessity of another approach for PTS problem is demonstrated in Fig. 3, where the scalar concentration at the wall is shown for two numerical experiments (realizations). The concentration represents the mixing of the injected ECC water (red color) with the primary water (blue) initially present in the cold leg and RPV. In these realizations, the same computational setup was used (i.e., the same mesh, initial and boundary conditions, time step, discretization schemes, LES model, etc.). Only a slightly different turbulent perturbation was applied at the ECC inlet, while maintaining the same turbulent intensity.

The figure clearly shows that two substantially different turbulent mixing patterns are developing in these numerical experiments. The same is happening in the physical experiments (see Fig. 7), since there will be also a difference in the fluctuations due to the turbulent nature of the flow in the ECC pipe. In the rest of this section three techniques are used to compare the results obtained on the different grids. The mixing characteristics of the flow in the cold leg and RPV are analyzed via examination of the scalar concentration.

A signal from a monitor point can be considered in the time domain using ensemble averaging. Ensemble averaging requires that a physical and/or numerical experiment has to be repeated a large number of times in order to provide adequate statistics, which is quite expensive. The simulations on grids **A**, **B** and **C** with different typical cell sizes have been performed five times (more details on this can be found in

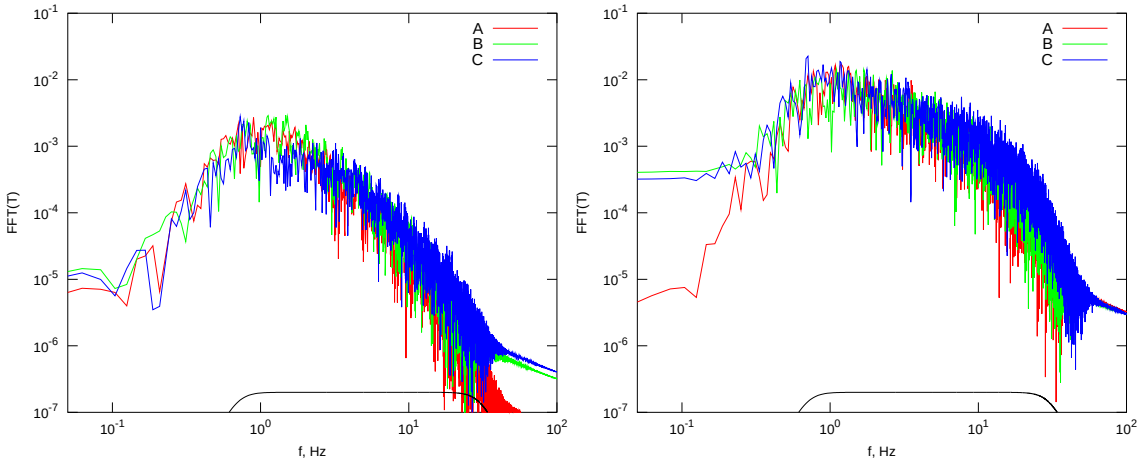

Figure 6: Power spectra for the scalar on the different meshes at the reactor inlet (left) and upper downcomer (right) sections.

[5]). The upper plot in Fig. 4 presents the ensemble averaged value of the concentration as a function of time for these grids, whereas the lower plot presents the corresponding RMS. Apparently, these three different grids give practically the same results for the ensemble mean as well as the ensemble RMS.

Another approach is demonstrated in Fig. 5, where the ensemble averaged data of grid **B** (green color) is compared to the individual realizations on grids **A-**, **A**, **C** and **C+**. The thick green shaded line represents the ensemble average $\pm$ ensemble RMS of the scalar on grid **B**. Any individual realization lies within the shaded region with 68.27% probability, provided that the ensemble has a normal distribution. Obviously, the results obtained on the different grids generally lie within these margins.

Finally, for the buoyancy-driven flow in the RPV, we apply analysis in the frequency domain [6]. The Fourier transformation is applied for the time series data, this results in complex-valued coefficient containing all the information about the series in terms of frequencies, amplitudes and phases. A spectrum is obtained by taking the magnitude of the coefficients. Since Fourier transformation implies periodicity of the signal, the given non-stationary signal was filtered by a fourth-order band-pass Butterworth filter. The results for the grids **A**, **B** and **C** are shown in Fig. 6. The simulations on all three grids predict the same magnitudes in the pass-band range shown by the line near the bottom of the plot. This indicates, that the subgrid scale model together with the numerical error does not affect the frequency content.

4 Validation against experiment

In the above case it was observed that the mixing in the downcomer is quite sensitive to small turbulent disturbances in the ECC injection pipe. Such differences were also found between individual experimental realizations obtained at the same conditions for the non-zero flow rates in the

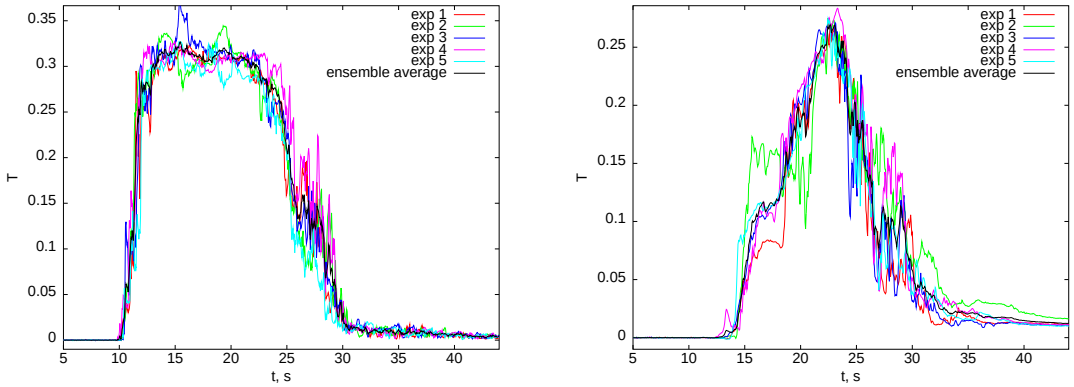

Figure 7: Time history of the scalar concentration near the wall for 5% flow rate, ensemble of five individual realizations (thin lines) and ensemble average (thick line) are plotted at monitor points in the reactor inlet (left) and upper downcomer (right) sections.

cold leg. Figure 7 shows an ensemble of five experimental realizations and average between them. The time histories of the scalar at near-wall monitor points from three sections are presented for the 5% case.

Evidently, the accuracy of LES for PTS cannot be directly quantified by comparison of a single numerical experiment with only one realization of the corresponding physical experiment. To resolve this validation issue, we perform comparison in four steps: qualitative comparison of a single experimental and numerical realization; application of ensemble averaging of the experimental data; analysis of the frequency spectra; engineering approach for comparison of local temperature drop. These steps will be explained in details through the subsequent paragraphs.

4.1 Qualitative comparison

A comparison of experimental and numerical results is presented in Figs. 8 and 9, where the scalar concentration is shown. A single experimental realization and the corresponding simulation are shown side by side for every flow rate. The data are normalized to the maximum value that has passed trough the given measurement section. The yellow and red colors indicate high concentration of the scalar and represent cold ECC water.

Instantaneous snapshots at the reactor inlet are shown in Fig. 8 for the times when ECC water is passing the section. The starting time and duration are different for every case because of the different bulk velocities. Evidently, no stable stratification can be observed in the experiment (upper row) and simulation (lower row) in all the cases. With increase of the flow rate, and consequently the Reynolds number Re, the mixing in the cold leg became more intensive. The time of cold water passage and the maximum values are predicted correctly in the simulation.

For the transient 3D cases, it is convenient to show the results in the downcomer using a so-called "unwrapped view" (Fig. 9). The scalar concentration is shown for all the sensors in the upper and

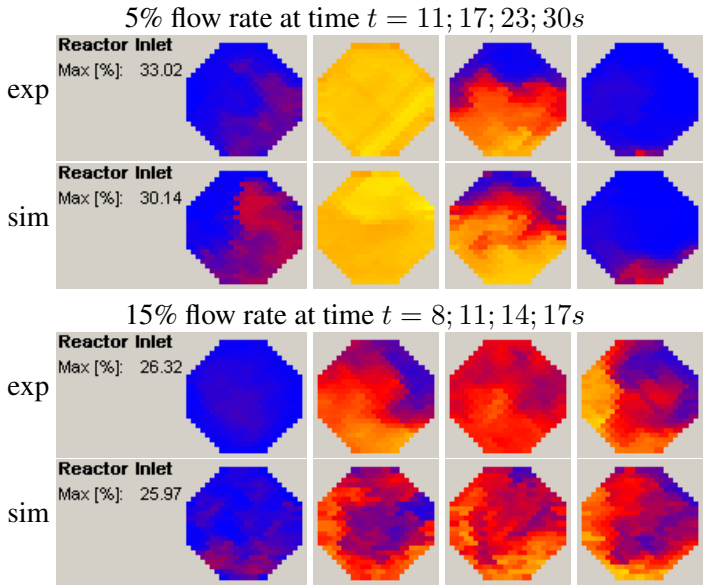

Figure 8: Scalar concentration at the reactor inlet position, experimental data are in the upper row.

lower downcomer positions in the circumferential direction for every time step. The red arrow at the top shows the position of the cold leg with the ECC injection, whereas the remaining black arrows correspond to the other cold leg connections. The presented experimental and numerical realizations are pretty much similar. That is, the ECC water in the simulation reaches the upper downcomer at the same time as in the experiment for all flow rates, and the maximum concentrations in the simulations are in good agreement with the experimental values. The typical patterns of buoyancy-driven, transitional, and momentum-driven flow regimes in the downcomer are also predicted correctly. In the first case, the colder ECC mixture streams almost vertically in the upper downcomer position, whereas spreading in the lateral direction occurs below. For the momentum-driven case, the circumferential spreading is already large in the upper downcomer position, and the colder water reaches the lower plenum from the opposite side of the RPV.

4.2 Ensemble averaging

While the simulations were performed once for every case, the experiments were repeated 3 or 5 times. So, from the experimental results, the ensemble average and ensemble RMS can be estimated. Figure 10 shows the time history of the scalar concentration for the 5% natural circulation flow rate in a monitor point. Within this figure, the simulation (thin red line) is compared with the ensemble average of the experimental realizations (thick black line), taking into account one ensemble RMS (thin vertical lines). Generally, the agreement is good considering that the thin vertical line covers every possible realization with a probability of 68.27% at best. The corresponding plots for the 10 and 15% flow rate gave similar results.

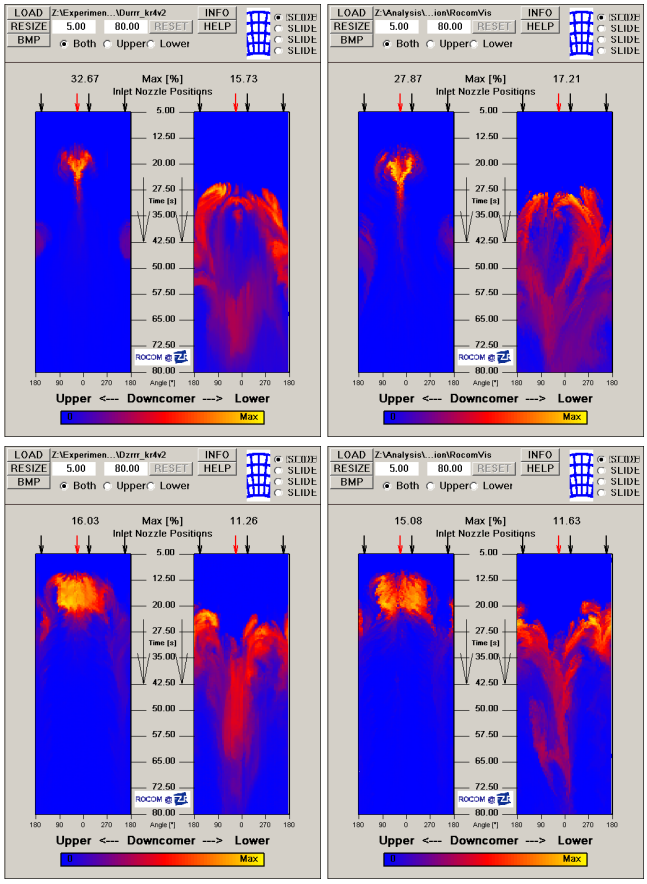

Figure 9: Unwrapped view of the scalar concentration at the downcomer positions for 5% (top) and 15% (bottom) flow rates. Experimental data are in the left column.

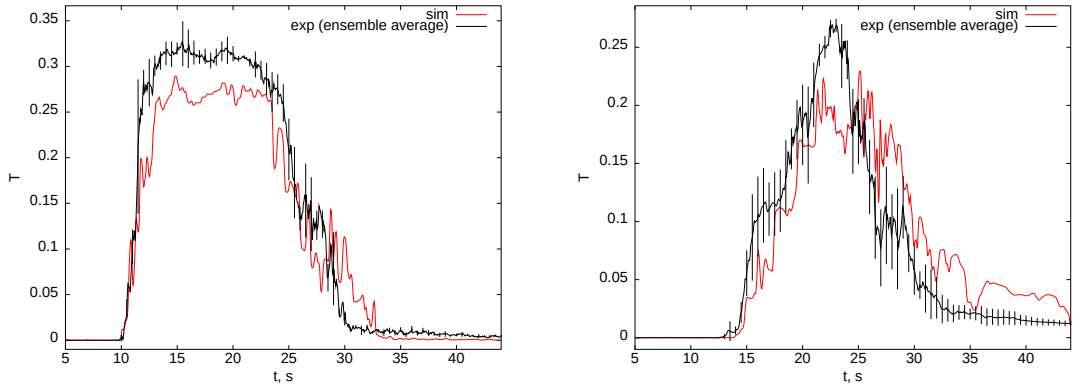

Figure 10: Time history comparison for 5% flow rate. The experiment (thick line) and simulation (thin) are plotted at monitor points in the reactor inlet (left) and upper downcomer (right) sections. Thin vertical lines denote the ensemble RMS.

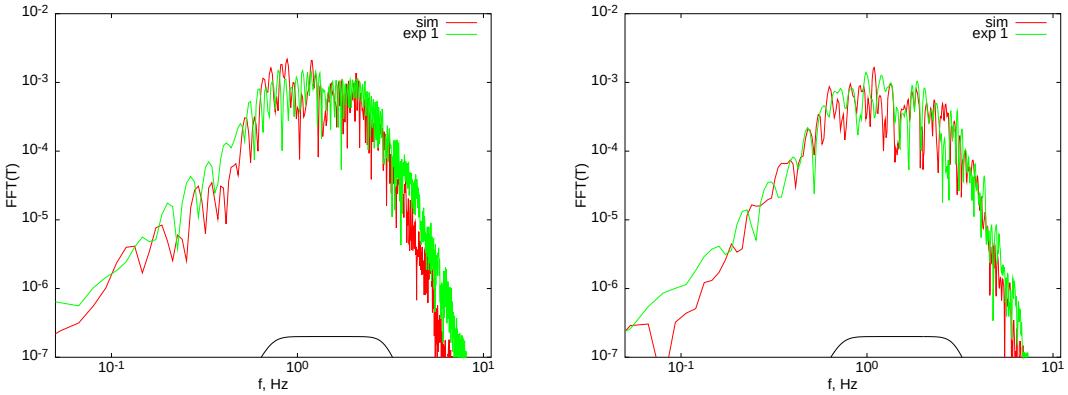

Figure 11: Power spectra of the experiment and simulation for 5% flow rate at monitor points in the reactor inlet (left) and upper downcomer (right) sections.

4.3 Frequency spectra

The relative importance of the fluctuations at the different frequencies can be assessed from a frequency spectrum. The spectra were obtained for single experimental and numerical realization as described earlier. A comparison of the spectra in Figs. 11 shows a good qualitative and quantitative agreement. This third validation step shows that LES can reproduce the spectrum of the turbulent fluctuations accurately for all considered cases.

4.4 Engineering approach

Temperature gradients in the RPV wall can have a strong influence on the structural behavior of the RPV. Such effects cannot be assessed directly from the considered ROCOM mixing tests. However, there is a direct relation between the induced temperature gradients in the walls and the sudden temperature drop of the coolant mixture in the downcomer during a PTS scenario. From an engineering perspective, the maximum temperature drop over time can be considered as a very important validation parameter. Therefore, it is analyzed in further detail.

In ROCOM, the maximum temperature drop over time at each location corresponds to the maximum value of the concentration $T_{\max}$ at each monitor point. These values are plotted along circumferential direction in Figs. 12. Only monitor points near the outer wall are taken. The data from all available experimental realizations (thin lines) are shown along with the numerical data (thick lines). The distribution of maximum concentrations is rather similar for the different realizations, and direct comparison with the simulation is possible. Evidently, the predicted values are very close to those observed in the experiment. A slight under-prediction is observed for 5% flow rate (Fig. 12, top). Generally, a conservative estimate of the temperature drop can be obtained from the numerical results with a safety factor of $1.1 - 1.3$.

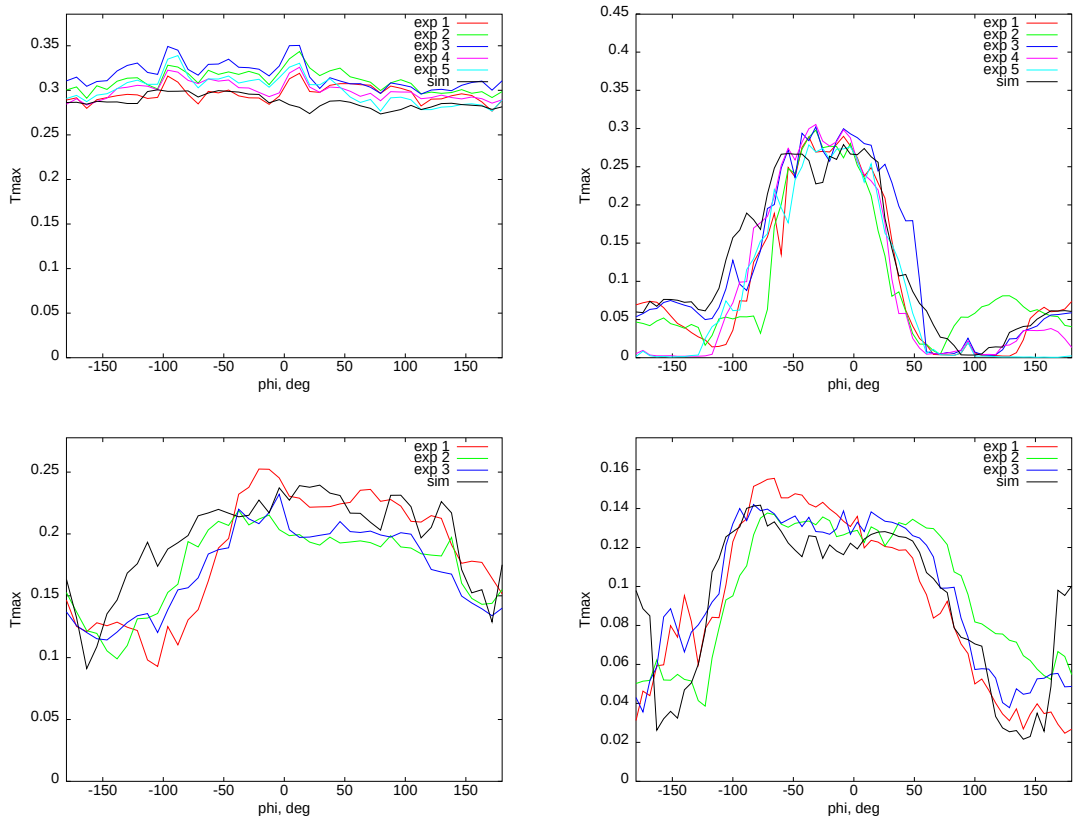

Figure 12: Distribution of maximum concentration near the wall for 5% (top) and 15% (bottom) flow rates at monitor points in the reactor inlet (left) and upper downcomer (right) sections.

5 Summary and conclusions

Large-eddy simulations are presented for three coolant mixing experiments that have been performed within the ROCOM test facility of Forschungszentrum Dresden-Rossendorf (FZD). These experiments correspond to a buoyancy driven, momentum driven, and a transitional regime. For all considered cases, the mixing in the downcomer is very sensitive to upstream turbulent disturbances. Therefore, the accuracy of the LES for this flow could not be directly quantified by conventional comparison of a single experiment with the corresponding simulation. To resolve this validation issue, the analysis has been performed in four steps using qualitative and quantitative comparison with experimental data in the time- and frequency-domain.

The following conclusions can be drawn with respect to accuracy of the LES application to a single-phase PTS problem:

- Mixing in the downcomer is quite sensitive to small turbulent disturbances in the injection of the cold ECC water into the cold leg, i.e., two simulations performed with slightly different fluctuations at the inlet result in substantially different flow in the downcomer;
- The computed coolant mixing is in a good agreement with the experimental one for the three considered flow regimes. The simulations reproduce the flow patterns correctly for all the considered regimes;
- The power spectra predicted by LES slightly over-estimate fluctuations for the 10% flow rate, it is probably caused by the transitional nature of this case. Otherwise, the qualitative and quantitative agreement is very good in terms of turbulent fluctuations.
- A conservative estimate of the temperature drop near the wall can be obtained from the numerical results with safety factor of $1.1 - 1.3$.
- Generally, the current simulations give a realistic and reliable description of the considered mixing experiments.

Acknowledgment

The authors are grateful to Pieter Wakker and Frederic Blom from NRG for valuable comments on this paper. The detailed experimental data together with helpful remarks are provided by Sören Kliem from FZD. This contribution is highly appreciated.

References

[1] Brian L. Smith. Identification and prioritization of generic nuclear safety problems requiring cfd analysis. In *17th International Conference on Nuclear Engineering*, 2009. Brussels, Belgium, July 12 – 16, 2009.

[2] Sander M. Willemsen and Jan-Aiso Lycklama á Nijeholt. Assessment of CFD modeling for PTS thermal-hydraulics using multiple scale experimental facilities. In *International Congress*

on Advances in Nuclear Power Plants (ICAPP), number 6259, 2006. June 4-8, 2006, Reno, Nevada, USA.

[3] U. Rohde, S. Kliem, T. Höhne, R. Karlsson, B. Hemström, J. Lillington, T. Toppila, J. Elter, and Y. Bezrukov. Fluid mixing and flow distribution in the reactor circuit, measurement data base. *Nuclear Engineering and Design*, 235(2–4):421 – 443, 2005.

[4] H. M. Prasser, A. Böttger, and J. Zschau. A new electrode-mesh tomograph for gas-liquid flows. *Flow Measurement and Instrumentation*, 9(2):111 – 119, 1998.

[5] M.S. Loginov, E.M.J. Komen, and A.K. Kuczaj. Application of large-eddy simulation to pressurized thermal shock problem. In *17th International Conference on Nuclear Engineering*, number 75894, 2009. Brussels, Belgium, July 12 – 16, 2009.

[6] M.S. Loginov, E.M.J. Komen, and A.K. Kuczaj. Application of large-eddy simulation to pressurized thermal shock problem: A grid resolution study. *Nuclear Engineering and Design*, 240(8):2034 – 2045, 2010.

[7] H.G. Weller, G. Tabor, H. Jasak, and C. Fureby. A tensorial approach to computational continuum mechanics using object orientated techniques. *Comput. Phys.*, 12(6):620 – 631, 1998.

[8] A.W. Vreman. An eddy-viscosity subgrid-scale model for turbulent shear flow: algebraic theory and applications. *Phys. Fluids*, 16(10):3670 – 3681, 2004.

[9] M. H. Baba-Ahmadi. *Construction of inlet conditions for large eddy simulation*. PhD thesis, University of Exeter, 2007.